Lattice dynamics and pressure-induced phase transitions in $Bi_2W_2O_9$: High-pressure Raman study

M. Maczka,[1] W. Paraguassu,[2] P. T. C. Freire,[3] A. G. Souza Filho,[3] J. Mendes Filho,[3] and J. Hanuza[4]
[1]*Institute of Low Temperature and Structure Research, Polish Academy of Sciences, P.O. Box 1410, 50-950 Wroclaw 2, Poland*
[2]*Departamento de Fisica, Universidade Federal do Maranhão, São Luis 65085-580, MA, Brazil*
[3]*Departamento de Fisica, Universidade Federal do Ceara, P.O. Box 6030, Fortaleza 60455-970, CE, Brazil*
[4]*Department of Bioorganic Chemistry, University of Economics, 53-345 Wroclaw, Poland*
(Received 28 December 2009; published 5 March 2010)

Lattice dynamics calculations and high-pressure Raman scattering study of $Bi_2W_2O_9$, which is an $m=2$ member of the cation-deficient bismuth layered Aurivillius family of compounds, are presented. These studies showed the onset of two reversible second-order phase transitions near 2.8 and 4.8 GPa. The pressure dependence of Raman bands provides strong evidence that the first phase transition involves the loss of the WO_6 tilt mode around pseudotetragonal axis. The second transition is likely related to some shift of the W atoms and/or tilting of the WO_6 octahedra plus shift of the Bi atoms or the whole Bi_2O_2 layers. In contrast to the $m=1$ cation-deficient bismuth layered compounds, Bi_2WO_6 and Bi_2MoO_6, no soft-mode behavior was observed for $Bi_2W_2O_9$ and the transition at 4.8 GPa leads to symmetry lowering.

DOI: 10.1103/PhysRevB.81.104301 PACS number(s): 78.30.Hv, 77.84.Bw, 77.80.B−

I. INTRODUCTION

Bismuth layered compounds (Aurivillius family) of general formula $(Bi_2O_2)(A_{m-1}B_mO_{3m+1})$ consist of alternating perovskitelike $A_{m-1}B_mO_{3m+1}$ slabs and fluoritelike Bi_2O_2 layers. The perovskitelike slabs may contain 1–8 layers ($m=1-8$).[1] This family of compounds have received much attention for device applications. For instance, these compounds are important candidates for the development of ferroelectric random access memories.[2–4] They constitute also an important class of oxide anion conductors.[1,5,6] Recently, $Bi_2W_2O_9$ was found to be a photocatalytic material for H_2 and O_2 evolution as well as photodegradation of organic compounds.[7,8] It was also found to be a promising material for microwave applications.[9]

In the case of $Bi_2W_2O_9$, no voluminous A cation is present on the cubo-octahedral sites of the W_2O_7 slabs.[10,11] Therefore, $Bi_2W_2O_9$ can be considered as the $m=2$ member of the family $(Bi_2O_2)(B^{VI}_mO_{3m+1})$ of cation-deficient Aurivillius phases.[10,11] Up till now only Bi_2MoO_6, Bi_2WO_6, and $Bi_2W_2O_9$ have been identified as belonging to this cation-deficient Aurivillius family.[11]

It is well known that all bismuth layered crystals have the same prototype I4/mmm structure and the distortion from this structure is induced by condensation of different displacive modes.[12–14] The most important displacive mode, which is responsible for ferroelectricity in the whole family of Aurivillius compounds, transforms according to the irreducible representation Γ_5^- (E_u) of I4/mmm.[12–14] The remaining modes correspond to rotations of the WO_6 octahedra along the twofold axis parallel to the [110] direction of the tetragonal phase or along the tetragonal axis.[12–14] $Bi_2W_2O_9$ exhibits the same type of distortion with respect to the prototype I4/mmm structure as $ABi_2Nb_2O_9$ (A=Ca,Sr,Pb).[11] However, the structure of $Bi_2W_2O_9$ is unique among bismuth layered materials, i.e., the direction of the cooperative displacement of the W atoms is *antiparallel* from one octahedral layer to the other and from one W_2O_7 slab to the other.[11] As a result, $Bi_2W_2O_9$ is nonferroelectric and it crystallizes with the $Pna2_1$ structure with $a=5.440$ Å, $b=5.413$ Å, and $c=23.740$ Å, whereas the $m=2$ ferroelectric niobates crystallize with the $A2_1am$ space group.[10–14] It is also worth noting that there are no reports on polymorphism of $Bi_2W_2O_9$.

Pressure-dependent studies of this large family of compounds are scarce. In particular, Raman-scattering studies under pressure were carried out only for $Na_{0.5}Bi_{4.5}Ti_4O_{15}$, $Bi_4Ti_3O_{12}$, Bi_2WO_6, and Bi_2MoO_6,[15–18] and no high-pressure studies have been yet undertaken for $Bi_2W_2O_6$. Published results show that high-pressure studies may provide very valuable information on origin of lattice instabilities in this family of compounds. For instance, they showed that $Na_{0.5}Bi_{4.5}Ti_4O_{15}$ and $Bi_4Ti_3O_{12}$ exhibit second-order phase transitions at about 1.94 GPa and near 3 GPa, respectively, which are accompanied by partial softening of a low-frequency mode upon approaching the phase-transition pressure, followed by hardening in the high-pressure phase.[15,16] They also showed that Bi_2MoO_6 (Bi_2WO_6) undergoes two phase transitions at 2.8 (3.4) GPa and 7.0 (6.2) GPa, respectively.[17,18] Similarly to $Na_{0.5}Bi_{4.5}Ti_4O_{15}$ and $Bi_4Ti_3O_{12}$, the first phase transition in Bi_2MoO_6 is associated with partial softening of the low-frequency mode but this mode disappears above 2.8 GPa.[18] In contrast to this behavior, the frequency of the soft mode observed in Bi_2WO_6 decreases to zero upon approaching the second phase transition.[17] Raman data also indicated that the pressure-induced structural changes in Bi_2MoO_6 are mainly related to the rigid rotations of MoO_6 octahedra and changes in the Bi_2O_2 layers.[18] In contrast to this behavior, distortion of the WO_6 octahedra significantly increases in Bi_2WO_6 upon increasing pressure.[17]

The above examples show that different bismuth layered crystals behave in a different way upon application of pressure, in spite of the same prototype I4/mmm structure. Therefore in order to improve the understanding of the nature of lattice instabilities in this family of compounds, it is necessary to access the properties of different members of

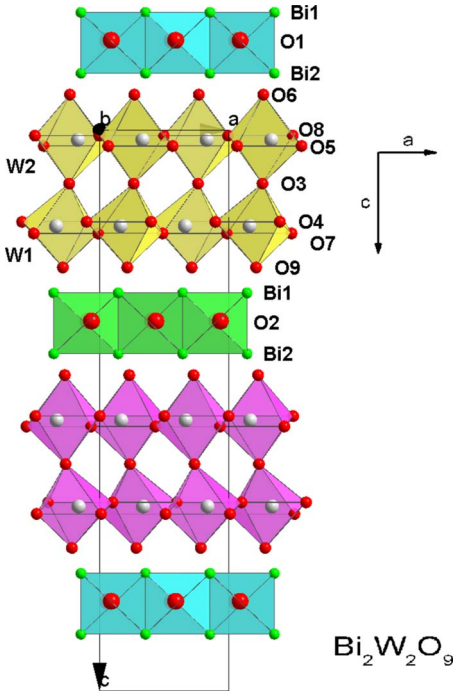

FIG. 1. (Color online) View of the $Bi_2W_2O_9$ crystal structure ($Pna2_1$) along the *b* axis.

Aurivillius family both as a function of temperature and pressure. This paper reports high-pressure Raman studies of $Bi_2W_2O_9$ single crystal. Our present results indicate that $Bi_2W_2O_9$ exhibits two structural transitions near 2.8 GPa and 4.8 GPa accompanied, respectively, by increasing and decreasing of symmetry. However, no soft-mode behavior associated with lattice instabilities could be observed.

II. EXPERIMENTAL

Single crystals of $Bi_2W_2O_9$ were grown by melting a mixture of $Bi_2W_2O_9 \cdot 10B_2O_3$ at 830 °C (polycrystalline $Bi_2W_2O_9$ was prepared by firing stoichiometric amounts of Bi_2O_3 and WO_3 oxides at 800 °C) in a platinum crucible, cooling it at the rate 1.2 C/h to 650 °C and then at the rate 5 °C/h to room temperature. The single crystals were separated from the B_2O_3 flux by washing with hot water.

The high-pressure Raman spectra were obtained with a triple-grating spectrometer Jobin Yvon T64000, equipped with a N_2-cooled charge-coupled device detection system. The line 514.5 nm of an argon laser was used as excitation. An Olympus microscope lens with a focal distance $f = 20.5$ mm and a numeric aperture of NA=0.35 was used to focus the laser beam on the sample surface. The high-pressure experiments were performed using a diamond anvil cell with a 4:1 methanol:ethanol mixture as the transmission fluid. Pressures were measured based on the shifts of the ruby R1 and R2 fluorescence lines. The spectrometer slits were set for a resolution of 2 cm^{-1}.

III. RESULTS AND DISCUSSION

A. Ambient pressure crystal structure of $Bi_2W_2O_9$

In order to understand the general behavior of $Bi_2W_2O_9$ crystal under pressure, it is important to provide a brief discussion of the crystal structure at ambient pressure and room temperature. This crystal is built up of alternating Bi_2O_2 layers and W_2O_7 slabs. At room temperature the structure is orthorhombic, $Pna2_1$, and the WO_6 octahedra are joined by the axial O3 and equatorial oxygen atoms O4, O5, O7, and O8 forming double W_2O_7 slabs (see Fig. 1). The axial oxygen atoms O6 and O9 connect the WO_6 octahedra to the BiO_6 polyhedra.[10,11] This orthorhombic structure can be regarded as derived from a high-symmetry body-centered tetragonal structure (space group symmetry I4/mmm). As emphasized by Champarnaud-Mesjard *et al.*[11] the orthorhombic distortion corresponds to cooperative antiparallel displacement of W atoms along the *a* axis, an important and symmetric tilting of the WO_6 octahedra with respect to the *b* axis, a slight antisymmetric tilting of the WO_6 octahedra with respect to the *a* axis, and a rotation of about 9° around the *c* axis, in the opposite sense from one octahedral layer to the other and from one W_2O_7 slab to the other.[11] The type of distortion with respect to the prototype I4/mmm structure is the same as for other $m=2$ Aurivillius phases but in the latter case all the shifts of the *B* atoms and all the tiltings and rotations of the octahedra are in the same sense.[11] As a consequence, the octahedral layers are related by the mirror

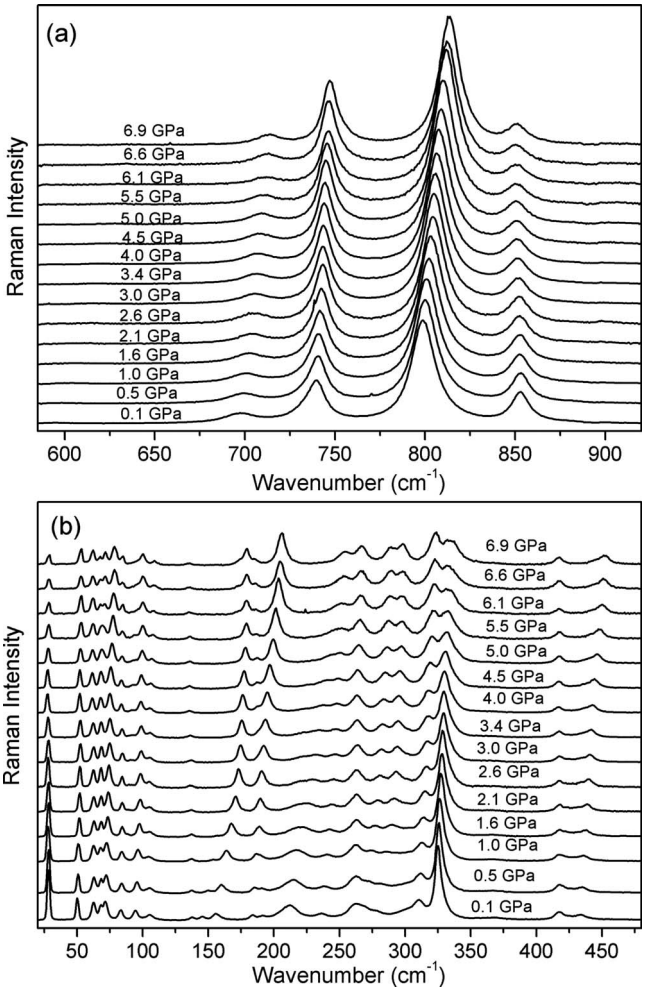

FIG. 2. Raman spectra of $Bi_2W_2O_9$ recorded at different pressures during compression experiments in the (a) high-wave-number and (b) low-wave-number regions.

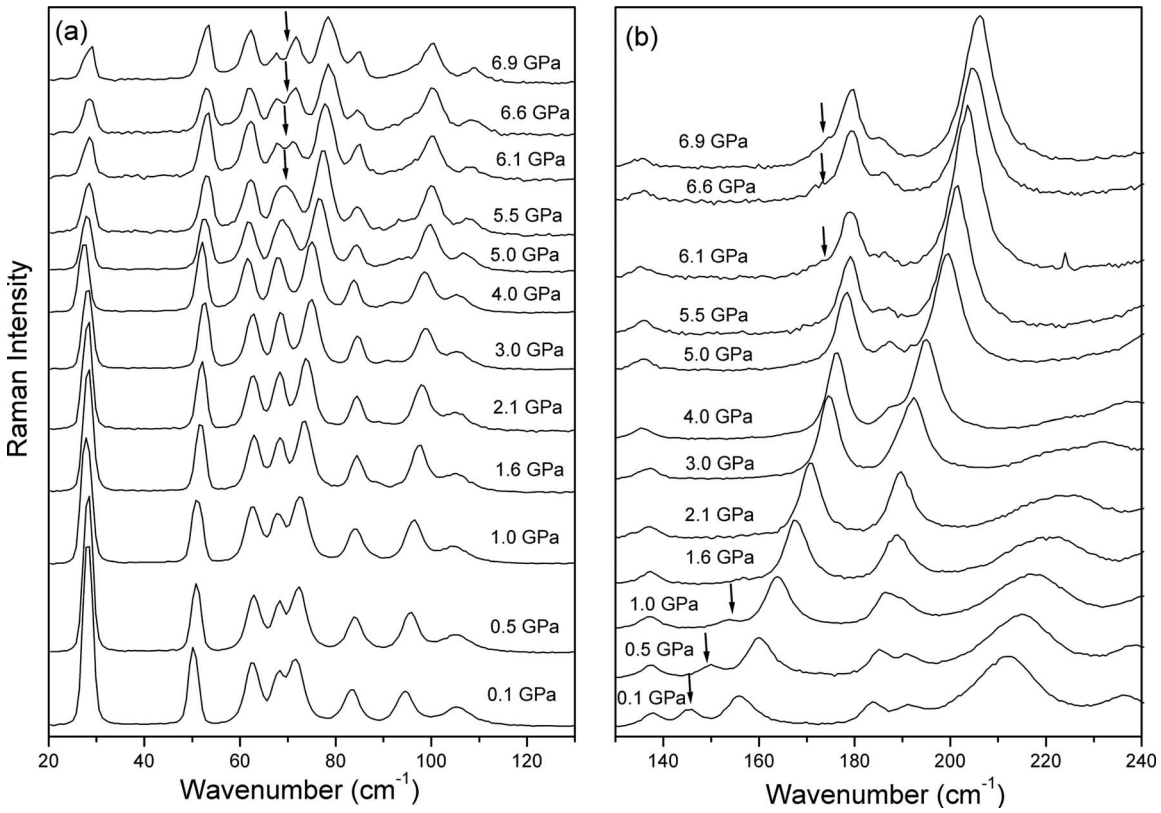

FIG. 3. Enlarged parts of the Raman spectra of Bi_2WO_6 in the 20–130 [panel (a)] and 130–240 cm^{-1} range [panel (b)] recorded at different pressures during compression. The arrows indicate bands, which appear, disappear or split under applied pressure.

plane for the $m=2$ Aurivillius phases but this mirror plane is lost for $Bi_2W_2O_9$ crystal. This leads to doubling of the primitive cell and number of phonon modes for $Bi_2W_2O_9$, in comparison with $m=2$ Aurivillius phases.

B. Lattice dynamics calculations and assignment of modes

A standard group theoretical analysis for the $Pna2_1$ ambient pressure phase of $Bi_2W_2O_9$ containing 52 atoms in the unit cell leads to 156 degrees of freedom at the Brillouin zone center (Γ point). The optical modes are distributed among the irreducible representations of the factor group C_{2v} as $38A_1+39A_2+38B_1+38B_2$. Selection rules state that A_1, B_1, and B_2 modes are both Raman and IR active whereas the A_2 modes are only Raman active.

Lattice dynamics (LD) calculations were performed using GULP code developed by Gale.[19] We have chosen a set of classical ionic pair potential that better optimize the $Bi_2W_2O_9$ structure ($Pna2_1$ space group). The obtained set of potential parameters has been then used to derive the initial force constants that were refined using Wilson's FG matrix method and the software package VIBRATZ developed by Dowty.[20]

The ionic shell model used in the GULP code treats the material as a collection of core-shell systems (symbolizing nuclei and electron shell) interacting to each other through electrostatic and short-range classic potentials. This model was successfully used for a number of molybdate- and tungstate-based systems.[21–23] The following interatomic potential is taken into account:

$$U_{ij}(r_{ij}) = \frac{z_i z_j e^2}{r_{ij}} + b_{ij} \exp\left[\frac{-r_{ij}}{\rho_{ij}}\right] - \frac{c_{ij}}{r_{ij}^6}. \quad (1)$$

The first term is related to the Coulomb forces for modeling the long-range interactions. The second term is related to the Born-Mayer-type repulsive interaction for accounting the short-range forces. A van der Waals attractive interaction (third term) models the dipole-dipole interaction. z_i and z_j are the effective charges of the i and j ions, respectively, separated by the distance r_{ij}. The parameters ρ_{ij} and b_{ij} correspond to the ionic radii and ionic stiffness, respectively. The initial lattice parameters and atomic positions for the $Bi_2W_2O_9$ structure were taken from the experimental data.[11] The potential parameters and ionic charges used in our cal-

TABLE I. Force constant values for $Bi_2W_2O_9$ crystal used in LD calculations.

Bonds	Force constant range mdyn/Å
Bi-O	0.4–0.6
O-O	0.35–0.45
W-O3	3.1
W-O6	3.6
W-O9	4.6
W-O5 and W-O8	1.37, 1.5
W-O4 and W-O7	1.53, 1.7

TABLE II. Experimental and calculated wave numbers for $Bi_2W_2O_9$ together with the proposed assignment.

Calculated				Experimental		
A_1	B_1	A_2	B_2	Raman	IR (Ref. 24)	Assignment
915.9	915.8	920.1	920.1		936 ± 1	WO_6 stretching modes
840.3	840.5	851.5	851.5	853.0 ± 0.1	855 ± 1	
774.8	774.5	784.0	784.0	799.0 ± 0.2	799 ± 2	
712.4, 683.6	712.4, 683.6	718.2, 712.1	718.2, 712.0	739.1 ± 0.1	759 ± 1	
632.1, 599.5	632.1, 599.5	686.9, 681.3	687.0, 681.3	698.1 ± 0.1	709 ± 1	
512.1	512.1	514.2, 508.3	514.2, 508.3	597.7 ± 0.5		Bi-O stretching modes
		492.7	492.7		550 ± 2	WO_6 bending modes
451.4	446.6	460.8	465.5			
		457.5, 452.4	456.9, 454.3	433.7 ± 0.2	435 ± 1	
	429.4	450.5	438.8	424.4 ± 0.9		
415.3			409.7	419.0 ± 0.7		
401.4	391.4	400.2		417.7 ± 0.1		
381.3, 356.5	378.0, 357.3	377.3, 357.5	376.1, 355.4	366.7 ± 0.1		Bi-O bending modes
338.2, 330.2	341.2, 334.9	337.1	342.3		337 ± 1	WO_6 and Bi-O bending modes and librations of WO_6
326.3, 320.5	327.3	331.4, 328.3	332.6, 324.8	325.2 ± 0.1		
309.7	315.9	318.3	306.9	310.4 ± 0.1		
295.5	311.8	298.4	301.7	301.3 ± 0.9		
283.9	294.1, 282.4	285.8	283.9, 280.1	279.2 ± 0.7	282 ± 2	
274.1, 271.9	274.9, 270.5	273.0		269.2 ± 0.4		
		261.9	262.1	262.0 ± 0.1		
255.7	255.8, 250.7				258 ± 1	
243.6	243.4	239.1	240.6	236.6 ± 0.2		
233.7	231.7			212.8 ± 0.3	217 ± 1	
214.0	217.3			207.6 ± 0.2		
		206.1	204.1	191.2 ± 0.1		
		174.9	175.0	183.6 ± 0.3		Translational motions of W atoms
167.0	160.6			156.8 ± 0.4	156 ± 1	
150.6	150.6	150.2	150.3	145.8 ± 0.5		
146.2	146.0	145.9	146.1	137.6 ± 0.1		
		121.1	120.4		117 ± 1	Translational motions of Bi and octahedral layers
101.3				105.3 ± 0.1		
91.2	96.2	91.1	92.2	95.0 ± 0.1	95 ± 1	
84.0	90.7	85.7	86.4	85.9 ± 0.1		
	84.7	83.8	82.7	84.3 ± 0.1		
74.8		75.2	69.3	71.7 ± 0.1		
66.7	69.1			68.1 ± 0.1		
	64.7	61.3	62.8	62.9 ± 0.1		
44.0	59.0	43.2	56.6		58 ± 1	
38.5	50.7	39.0	40.8	50.4 ± 0.1		RL mode
28.5	37.2	29.2		28.2 ± 0.1		RL mode

culation were the same as those reported by Islam *et al.*[1] for Bi_2WO_6. By using this set of parameters, a good agreement between the calculated and experimental lattice parameters was obtained with volumetric error within 1%.

The initial force constants were obtained by using the relation

$$f_{ij} = -\frac{1}{r}\frac{\partial U_{ij}(r)}{\partial r}, \tag{2}$$

where the indices i and j refer to interacting ions (first neighbors only) and r is the distance between them. The obtained force constant values were refined in order to better fit the

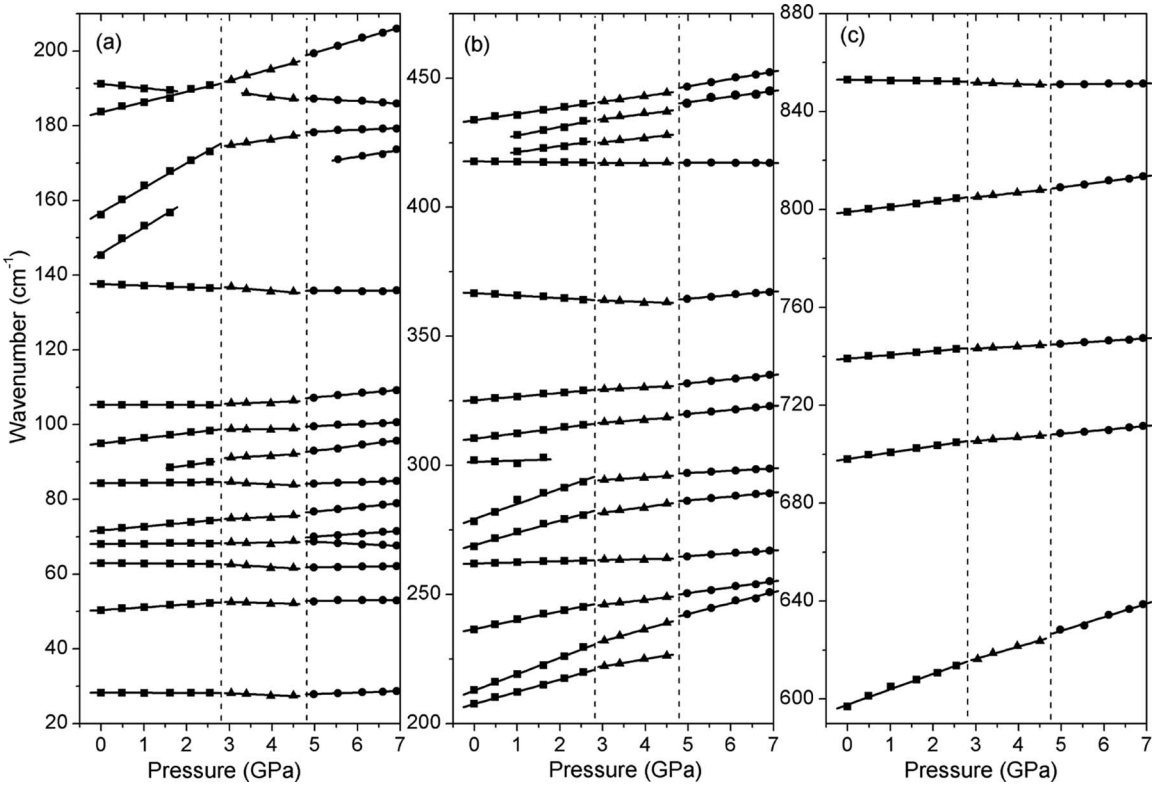

FIG. 4. Wave number vs pressure plots of the Raman modes observed in $Bi_2W_2O_9$ crystal for compression experiment. Uncertainties in phonon wave numbers are smaller than size of the symbols. The vertical lines indicate the pressures at which $Bi_2W_2O_9$ undergoes phase transitions. The solid lines are linear fits on the data to $\omega(P)=\omega_0+\alpha P$.

experimental data. The final values used in the calculations are listed in Table I and the calculated and experimental Raman and IR wave numbers are collected in Table II.

The Raman spectrum at room temperature and near ambient pressure (0.1 GPa) is shown in Fig. 2. The number of observed modes is smaller than expected for the $Pna2_1$ structure because the factor group splitting is very small for majority of modes. LD calculations show that modes in the 698–936 cm^{-1} range can be assigned to stretching modes of the WO_6 octahedra. The broad wave-number range in which the stretching modes are observed indicates that the WO_6 octahedra are strongly distorted. This conclusion is consistent with the ambient pressure x-ray diffraction studies.[11] The mode at 936 cm^{-1} corresponds to motions of mainly O3 oxygen atoms whereas the modes at 855 and 799 cm^{-1} involve mainly motions of the shorter (O9) and longer (O6) apical oxygen atoms, respectively. The atomic motions are in the direction nearly perpendicular to the layers. The modes in the 698–759 cm^{-1} range are due to asymmetric stretching modes of the WO_6 octahedra, involving motions of the equatorial oxygen atoms within layers (O_{eq}, oxygen atoms O4, O5, O7, and O8 in Fig. 1). Our calculations also show that the weak Raman band at about 598 cm^{-1} should be assigned to stretching mode of the BiO_6 polyhedra.

Bending modes of the WO_6 and BiO_6 units as well as librational modes of the WO_6 octahedra contribute to the bands observed in the 190–550 cm^{-1} range. Our calculations show that the main contribution to the IR mode at 550 cm^{-1} comes from the bending motions of the W-O bonds in the direction perpendicular to the layers. The modes in the 417–435 cm^{-1} range correspond mainly to bending modes of the WO_6 octahedra and the 367 cm^{-1} band has predominant contribution of Bi-O bending motions in the direction nearly perpendicular to the layers. The modes in the 190–337 cm^{-1} range can be assigned to bending modes of the WO_6 octahedra involving large motions of the equatorial oxygen atoms mainly. However, the modes in the 279–337 cm^{-1} range have also significant contribution of Bi-O bending motions and the modes in the 191–282 cm^{-1} range involve strong contribution of WO_6 librational motions along the c axis.

Translational modes are observed below 190 cm^{-1}. Since the $Bi_2W_2O_9$ structure is layered, some translational motions can be regarded as motions of the whole Bi_2O_2 layers and W_2O_7 slabs as rigid units. Such modes are called rigid layer (RL) modes. LD calculations for I4/mmm phase of $SrBi_2Ta_2O_9$, Bi_2WO_6, and $Bi_4Ti_3O_{12}$ revealed that the unstable, lowest frequency E_u translational mode can be described as a RL mode since it mainly involves movements of the Bi_2O_2 layers relative to the perovskitelike slabs.[13] Our LD calculations for orthorhombic $Bi_2W_2O_9$ show that the modes at about 28 and 50 cm^{-1} can be assigned to the RL modes since they involve movements of the Bi_2O_2 layers relative to the W_2O_7 slabs in the direction parallel to the layers. Our LD calculations also show that the modes in the 58–117 cm^{-1} range correspond to translational motions of the Bi atoms and larger fragments of the W_2O_7 slabs. Translations of the W atoms contribute to the modes observed in

TABLE III. Raman wave numbers ω_0 for the three phases of $Bi_2W_2O_9$ along with pressure coefficients α obtained from the linear fits on the data to $\omega(P)=\omega_0+\alpha P$.

Ambient pressure phase		Intermediate phase		High-pressure phase	
ω_0 (cm^{-1})	α (cm^{-1} GPa^{-1})	ω_0 (cm^{-1})	α (cm^{-1} GPa^{-1})	ω_0 (cm^{-1})	α (cm^{-1} GPa^{-1})
853.0 ± 0.1	−0.3 ± 0.1	853.4 ± 0.2	−0.5 ± 0.05	850.4 ± 0.3	0.1 ± 0.05
799.0 ± 0.2	2.2 ± 0.1	799.3 ± 0.2	1.9 ± 0.1	797.6 ± 0.8	2.3 ± 0.1
739.1 ± 0.1	1.5 ± 0.1	740.5 ± 0.1	0.9 ± 0.02	739.3 ± 0.5	1.2 ± 0.1
698.1 ± 0.1	2.6 ± 0.1	701.2 ± 0.4	1.4 ± 0.1	700.5 ± 1.0	1.6 ± 0.1
597.7 ± 0.5	6.3 ± 0.3	601.4 ± 1.5	5.0 ± 0.3	599.9 ± 2.4	5.6 ± 0.4
433.7 ± 0.2	2.4 ± 0.1	434.2 ± 0.2	2.2 ± 0.1	432.4 ± 0.7	2.9 ± 0.1
424.4 ± 0.9	3.4 ± 0.4	427.9 ± 1.3	2.1 ± 0.3	429.7 ± 2.2	2.2 ± 0.3
419.0 ± 0.7	2.4 ± 0.4	419.7 ± 0.8	1.8 ± 0.2		
417.7 ± 0.1	−0.2 ± 0.03	416.9 ± 0.7	0.1 ± 0.1	417.5 ± 0.2	−0.1 ± 0.03
366.7 ± 0.1	−1.0 ± 0.1	365.6 ± 1.1	−0.6 ± 0.2	357.6 ± 0.7	1.4 ± 0.1
325.2 ± 0.1	1.4 ± 0.1	327.0 ± 0.3	0.8 ± 0.1	323.6 ± 0.6	1.6 ± 0.1
310.4 ± 0.1	2.1 ± 0.1	312.7 ± 0.8	1.3 ± 0.2	312.2 ± 0.1	1.5 ± 0.1
301.3 ± 0.9	0.5 ± 0.6				
279.2 ± 0.7	5.9 ± 0.4	291.3 ± 0.4	1.0 ± 0.1	292.5 ± 0.5	0.9 ± 0.1
269.2 ± 0.4	4.7 ± 0.2	274.8 ± 1.0	2.3 ± 0.2	278.8 ± 0.6	1.5 ± 0.1
262.0 ± 0.1	0.4 ± 0.04	262.4 ± 1.0	0.3 ± 0.2	259.2 ± 0.3	1.1 ± 0.05
236.6 ± 0.2	3.4 ± 0.1	240.1 ± 0.3	2.0 ± 0.1	239.0 ± 0.8	2.3 ± 0.1
212.8 ± 0.3	6.4 ± 0.2	217.9 ± 0.5	4.7 ± 0.1	221.3 ± 2.3	4.2 ± 0.4
207.6 ± 0.2	4.7 ± 0.1	213.8 ± 0.4	2.8 ± 0.1		
191.2 ± 0.1	−1.1 ± 0.1	193.2 ± 1.7	−1.4 ± 0.4	190.6 ± 0.5	−0.7 ± 0.08
183.6 ± 0.3	2.8 ± 0.2	182.7 ± 0.5	3.1 ± 0.1	182.5 ± 0.6	3.4 ± 0.1
156.8 ± 0.4	6.6 ± 0.2	169.8 ± 0.4	1.7 ± 0.1	176.0 ± 0.7	0.5 ± 0.1
145.8 ± 0.5	7.0 ± 0.5			160.8 ± 2.2	1.8 ± 0.3
137.6 ± 0.1	−0.4 ± 0.03	139.4 ± 1.0	−0.9 ± 0.2	135.9 ± 0.4	0.0 ± 0.07
105.3 ± 0.1	0.0 ± 0.03	104.4 ± 0.8	0.4 ± 0.2	102.2 ± 0.3	1.0 ± 0.05
95.0 ± 0.1	1.4 ± 0.05	98.4 ± 0.6	0.1 ± 0.1	96.9 ± 0.3	0.5 ± 0.06
85.9 ± 0.1	1.6 ± 0.03	89.2 ± 0.6	0.6 ± 0.1	85.7 ± 0.4	1.5 ± 0.1
84.3 ± 0.1	0.1 ± 0.01	86.1 ± 0.7	−0.5 ± 0.1	82.5 ± 0.2	0.3 ± 0.03
71.7 ± 0.1	1.0 ± 0.05	73.3 ± 0.8	0.5 ± 0.1	71.0 ± 0.3	1.1 ± 0.04
				66.0 ± 0.1	0.8 ± 0.02
68.1 ± 0.1	0.1 ± 0.06	67.9 ± 1.3	0.1 ± 0.2	71.4 ± 0.3	−0.6 ± 0.05
62.9 ± 0.1	−0.1 ± 0.02	64.6 ± 0.8	−0.7 ± 0.2	61.0 ± 0.1	0.2 ± 0.02
50.4 ± 0.1	0.7 ± 0.06	53.4 ± 0.5	−0.3 ± 0.1	52.1 ± 0.5	0.1 ± 0.05
28.2 ± 0.1	0.0 ± 0.02	29.5 ± 0.7	−0.5 ± 0.2	25.9 ± 0.1	0.4 ± 0.02

137–184 cm^{-1} range. It is worth noting that many low-wave-number modes have very small bandwidths (some even near 2 cm^{-1}). Such small bandwidths point to low anharmonicity of these modes.

C. High-pressure Raman scattering studies

Once a clear picture of the vibrational properties of $Bi_2W_2O_9$ is obtained we next discuss the effects of hydrostatic pressure on the structural and vibrational properties of this compound. Pressure dependence of Raman spectra is presented in Figs. 2 and 3. However, the overall changes in the Raman spectra can be better followed by analyzing the wave number (ω) vs pressure (P) plot shown in Fig. 4. Figure 4 shows that the pressure dependence of all vibrational modes can be well described using a linear function $\omega(P)=\omega_0+\alpha P$. The values of ω_0 and α are collected in Table III. By increasing pressure wave numbers of majority of modes increase (see Figs. 2–4). However, a few modes exhibit negative pressure dependence. For instance, negative pressure dependence is observed for the 191.2 cm^{-1} mode (at ambient pressure), which shifts to 179.2 cm^{-1} at 6.9 GPa. As a result of the opposite pressure dependence the modes at 191.2 and 183.6 cm^{-1} exhibit interesting crossover behavior.

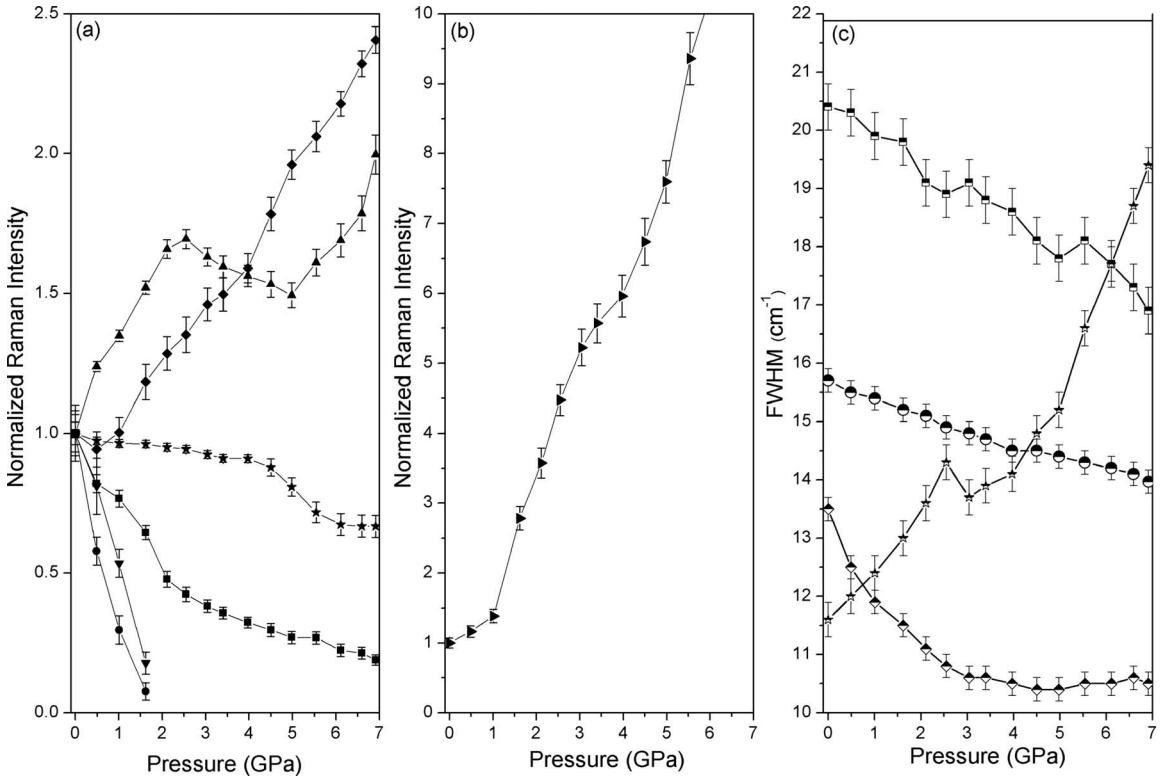

FIG. 5. (a) Pressure dependence of the integral intensity normalized for $P=0.1$ GPa for the 28.2 (squares), 145.8 (circles), 156.8 (up triangle), 301.3 (down triangle), 310.4 (diamonds), and 325.2 cm^{-1} bands (stars). Panel (b) presents pressure dependence of the integral intensity normalized for $P=0.1$ GPa for the 183.6 cm^{-1} band. Pressure dependence of FWHM of the Raman bands observed at 853.0 (stars), 799.0 (circles), 739.1 (diamonds), and 698.1 cm^{-1} (squares) are presented in panel (c). Solid lines are to guide the eyes.

It is worth noting that very similar crossover behavior was observed previously by us for the 208 and 186 cm^{-1} modes of Bi_2WO_6.[17] Figures 2–4 also show that in contrast to Bi_2WO_6, which showed a very clear soft-mode behavior, any of the low-wave-number modes of $Bi_2W_2O_9$ exhibit significant softening with increasing pressure. Raman study also reveals that intensities of a number of bands decrease continuously upon increasing pressure. This behavior is observed for the bands at 28.2, 207.6, 212.8, and 325.2 cm^{-1} (see Figs. 2 and 5). Significant intensity increase is observed for the bands at 68.1, 156.8, and 183.7 cm^{-1}.

When pressure reaches about 2.8 GPa, the 145.8 and 301.3 cm^{-1} bands disappear (see Figs. 3 and 5). Furthermore, a very clear change in the slope of wave number vs pressure is observed near 2.8 GPa. Clear anomalies near 2.8 GPa are also observed in the plots of full width at half maximum (FWHM) as a function of pressure for the stretching modes at 853.0 and 739.1 cm^{-1} [see Fig. 5(c)]. Figure 5(a) also shows that the normalized Raman intensity of the 156.8 cm^{-1} band increases up to 2.8 GPa followed by weak decrease up to about 5 GPa and increase at higher pressures. These modifications of the Raman spectra indicate that a continuous transformation takes place in $Bi_2W_2O_9$ near 2.8 GPa. By further increasing pressure, the band near 68 cm^{-1} exhibits splitting into two components at about 4.8 GPa [see Figs. 3(a) and 4]. This splitting is accompanied by a weak change in the slope of wave number vs pressure. Furthermore, a new band appears at about 171 cm^{-1} and two weak bands at 226 and 428 cm^{-1} are not observed above 4.8 GPa. Our results also show clear anomalies in intensities of the 156.8 and 325.2 cm^{-1} bands near 5 GPa. This behavior is very clearly observed in the plots of normalized intensity as a function of pressure [see Fig. 5(a)]. The discussed modifications indicate that $Bi_2W_2O_9$ exhibits another structural transformation at about 4.8 GPa associated with some subtle changes in the crystal structure.

In order to get more insight into the mechanism of phase transitions in $Bi_2W_2O_9$ we have also performed Raman studies of $Bi_2W_2O_9$ crystal during the decompression. Upon releasing pressure the spectrum of the starting orthorhombic phase was recovered, as can be observed in Fig. 6, thus indicating the reversibility of the process.

D. Pressure-induced phase transitions

Figures 2 and 4 show that all modes above 400 cm^{-1} exhibit very weak change in the slope of wave numbers vs pressure at the phase transitions. Furthermore, the Raman bands above 400 cm^{-1} also exhibit weak changes in relative intensities with pressure. However, significant changes in slopes and intensities are observed for many modes below 400 cm^{-1}. It is well known that the correlation lengths of the high-wave-number modes are on the order of a few angstroms whereas the low-wave-number modes are sensitive to long-range order. Our Raman results indicate, therefore, that phase transitions at 2.8 and 4.8 GPa are not accompanied by any significant distortion of the WO_6 octahedra but they lead to significant change in long-range order. As mentioned

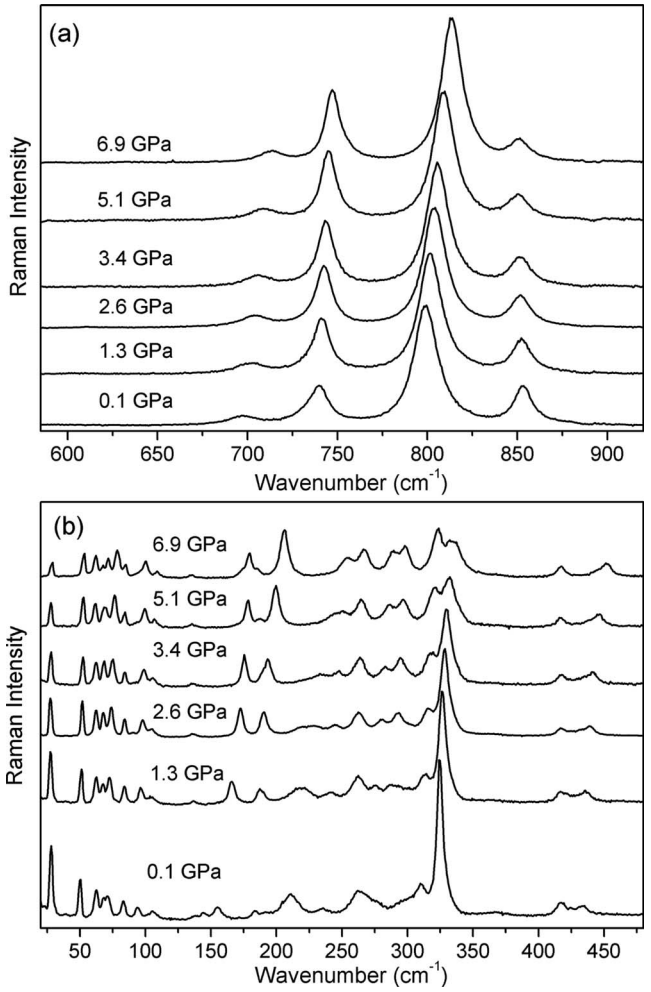

FIG. 6. Raman spectra of $Bi_2W_2O_9$ recorded at different pressures during decompression experiments in the (a) high-wave-number and (b) low-wave-number regions.

above the characteristic changes at 2.8 GPa are: (i) disappearance of the 145.8 and 301.3 cm^{-1} modes, (ii) very clear changes in the slope of wave numbers vs pressure (especially for the 279.2, 269.2, and 156.8 cm^{-1} modes), (iii) clear anomalies in the FWHM for the stretching modes at 853.0 and 739.1 cm^{-1}, and (iv) change in the slope of the normalized integrated intensity ratio for the 156.8 cm^{-1} band vs pressure. The disappearance of the two modes indicates that symmetry of the phase stable in the 2.8–4.8 GPa increases. Since the mode at 145.8 cm^{-1}, which disappears at 2.8 GPa, and the mode at 156.8 cm^{-1}, which exhibits strong change in the slopes, correspond to translational motions of the W atoms, the driving force of the phase transition at 2.8 GPa is most likely displacement of the W atoms. It is worth noting, however, that significant changes in the slope of wave numbers vs pressure at 2.8 GPa are also observed for the 279.2 and 269.2 cm^{-1} modes, which can be attributed to librations of the WO_6 octahedra along the *c* axis coupled with the bending modes of these units. Moreover, the band at 301.3 cm^{-1}, which disappears at 2.8 GPa, corresponds to the WO_6 bending mode. These facts suggest that the displacement of the W atoms is also associated with changes in rotation and/or tilting of the WO_6 octahedra, i.e., librations of the WO_6 octahedra also play very important role in the phase transition. As discussed above, one of the characteristic features of $Bi_2W_2O_9$ structure is an important and symmetric tilting of the WO_6 octahedra with respect to the *b* axis. This tilting is very similar to that observed for other $m=2$ Aurivillius phases such as, for instance, $SrBi_2Ta_2O_9$ and it corresponds to condensation of the Bmab displacive mode (or Cmca in the standard setting) transforming according to the irreducible representations X_3^- of I4/mmm.[14] Theoretical studies of $SrBi_2Ta_2O_9$ showed that the octahedral tiltings associated with the frozen X_3^- mode will tend to increase under pressure.[14] It is therefore very likely that our observed symmetry enhancement for $Bi_2W_2O_9$ is not related to this mode. Other characteristic features of the $Bi_2W_2O_9$ structure are a slight antisymmetric tilting of the WO_6 octahedra with respect to the *a* axis and a rotation of about 9° around the *c* axis. Our previous studies of orthorhombic ferroelectric phase of Bi_2WO_6, which has very similar degree of rotation around the *c* axis, showed that application of an external pressure resulted in decrease in this rotation.[17] When pressure reached 3.4 GPa, this distortion was lost. Interestingly, similarly as in case of $Bi_2W_2O_9$, very strong pressure dependence was observed for the mode near 140 cm^{-1} (corresponding to the 156.8 cm^{-1} mode of $Bi_2W_2O_9$) below 3.4 GPa followed by weak pressure dependence above 3.4 GPa. Moreover, as mentioned above strong changes are also observed for the 279.2 and 269.2 cm^{-1} modes involving large contribution of librational motions along the *c* axis. It is, therefore, plausible to assume that the phase transition at 2.8 GPa in $Bi_2W_2O_9$ is also associated with loss of the tilt mode around the *c* axis and symmetry of the phase stable between 2.8 and 4.8 GPa is still orthorhombic.

Figure 4 shows that the pressure dependence of wave numbers is very weak between 2.8 and 4.8 GPa for majority of modes. This result indicates that the intermediate phase is less compressible than the ambient pressure phase. Interestingly, many modes below 140 cm^{-1} exhibit weak negative pressure dependence (see Table III). The softening of modes under pressure reveals that the anharmonicity becomes important and it is an indication of some crystal instability. When the pressure reaches 4.8 GPa, a phase transition takes place. Splitting of the band near 68 cm^{-1} and appearance of a weak band at about 171 cm^{-1} suggest symmetry decrease above 4.8 GPa. However, our spectra also show that two weak bands at 226 and 428 cm^{-1} are no longer observed above 4.8 GPa. This behavior can be most likely attributed to strong decrease in intensity and increase in bandwidth for these bands upon pressure. As can be noticed, the most pronounced change (splitting) occurs for the 68 cm^{-1} band. Furthermore, intensity of the 325.2 cm^{-1} bands shows clear anomaly near 5 GP. Raman data also show that intensity of the 183.6 cm^{-1} band strongly increases upon application of pressure in the whole pressure range studied. As mentioned above, the 325.2 and 183.6 cm^{-1} bands correspond to bending of the WO_6 octahedra and translations of the W atoms, respectively. The mode near 68 cm^{-1} corresponds to coupled motions of the W_2O_7 slabs and Bi atoms. The pressure dependence of the observed modes indicates, therefore, that the transition at about 4.8 GPa is likely related to some changes in the shifts of the W atoms and/or tilting of the WO_6 octa-

hedra. Since, however, the mode at 68 cm^{-1} has also significant contribution of the translational motions of the Bi atoms, we cannot exclude that this transition is also associated with shift of the Bi atoms or the whole Bi_2O_2 layers. Table III shows that many modes still exhibit large pressure dependence above 4.8 GPa, with α parameters up to 5.6 cm^{-1} GPa^{-1}. This result indicates that the high-pressure phase of $Bi_2W_2O_9$ is still a relatively soft material. High compressibility can be related to lack of voluminous cation on the cubo-octahedral sites of the W_2O_7 slabs.

Let us now shortly discuss the pressure dependence of the bandwidths for the stretching modes of the WO_6 octahedra. In the high-pressure experiments, increase in bandwidths is usually observed upon increasing pressure due to pressure gradient or slight nonhydrostaticity and creation of defects in a crystal. Interestingly, in the case of $Bi_2W_2O_9$ the bandwidths of the stretching modes observed at 799.0, 739.1, and 698.1 cm^{-1} decrease upon increase in pressure [see Fig. 5(c)]. The only exception is the 853.0 cm^{-1} band, which shows bandwidth increase. First of all, it is worth noting that the bandwidths of the discussed bands are large at ambient pressure and room temperature [see Fig. 5(c)]. Our LD calculations show that the large bandwidths can be most likely attributed to the fact that each of these bands is composed of a few Davydov components of similar energy (see Table II). Therefore, one of the possible explanations of the observed bandwidth decrease upon application of external pressure is enhancement of symmetry, which in turn may lead to decrease in the Davydov splitting. However, the 799.0 and 739.1 cm^{-1} modes show further decrease in bandwidths upon pressure also for the high-pressure phases, in spite of symmetry decrease at the 4.8 GPa phase transition. We suppose therefore that the pressure dependence of the bandwidths can also be related, at least partially, to the redistributions of the anharmonic couplings between the different phonon modes with pressure.

IV. CONCLUSIONS

Lattice dynamics calculations and high-pressure Raman studies were performed on $Bi_2W_2O_9$. Our results showed that the Raman spectra of $Bi_2W_2O_9$ are much more complex than the spectra of Bi_2WO_6 or $m=2$ Aurivillius compounds due to larger distortion of the octahedral slabs and lower symmetry. Pressure-dependent studies revealed successive pressure-induced second-order phase transitions at around 2.8 and 4.8 GPa. They have shown that the WO_6 octahedra are rigid entities and the first transition is most likely associated with the loss of the octahedral tilt mode around the pseudotetragonal axis. The second transition in $Bi_2W_2O_9$ is likely related to shift of the W atoms and/or tilting of the WO_6 octahedra plus shift of the Bi atoms or the whole Bi_2O_2 layers. This transition leads to symmetry lowering and no soft mode could be observed. In contrast to this behavior, symmetry enhancement was observed for Bi_2WO_6 and Bi_2MoO_6. Moreover, the second transition in Bi_2WO_6 was related to disappearance of the soft mode that corresponds most likely to the polar E_u mode responsible for ferroelectricity in all Aurivillius-type compounds.

ACKNOWLEDGMENTS

This work was supported by the Ministry of Science and Higher Education under Grant No. N N209 097335. The Brazilian authors acknowledge CNPq for grants.

[1] M. S. Islam, S. Lazure, R. N. Vannier, G. Nowogrocki, and G. Mairesse, J. Mater. Chem. **8**, 655 (1998).
[2] X. Mao, W. Wang, X. Chen, and Y. Lu, Appl. Phys. Lett. **95**, 082901 (2009).
[3] C. A. Paz de Araujo, J. D. Cuchiaro, L. D. McMillan, M. C. Scott, and J. F. Scott, Nature (London) **374**, 627 (1995).
[4] Y. Noguchi, K. Murata, and M. Miyayama, Appl. Phys. Lett. **89**, 242916 (2006).
[5] K. R. Kendall, C. Navas, J. K. Thomas, and H. C. zur Loye, Chem. Mater. **8**, 642 (1996).
[6] N. Kim, R. N. Vannier, and C. P. Grey, Chem. Mater. **17**, 1952 (2005).
[7] A. Martinez-de la Cruz, S. O. Alfrao, L. M. Torres-Martinez, and I. J. Ramirez, J. Ceram. Proc. Res. **9**, 490 (2008).
[8] J. Tang and J. Ye, J. Mater. Chem. **15**, 4246 (2005).
[9] A. Feteira and D. C. Sinclair, J. Am. Ceram. Soc. **91**, 1338 (2008).
[10] Y. Bando, A. Watanabe, Y. Sekikawa, M. Goto, and S. Horiuchi, Acta Crystallogr., Sect. A: Cryst. Phys., Diffr., Theor. Gen. Crystallogr. **35**, 142 (1979).
[11] J. C. Champarnaud-Mesjard, B. Frit, and A. Watanabe, J. Mater. Chem. **9**, 1319 (1999).
[12] Yu. E. Kitaev, M. I. Aroyo, and J. M. Perez-Mato, Phys. Rev. B **75**, 064110 (2007).
[13] R. Machado, M. G. Stachiotti, R. L. Migoni, and A. H. Tera, Phys. Rev. B **70**, 214112 (2004).
[14] J. M. Perez-Mato, M. Aroyo, A. Garcia, P. Blaha, K. Schwarz, J. Schweifer, and K. Parlinski, Phys. Rev. B **70**, 214111 (2004).
[15] J. Liu, C. Gao, G. Zou, and Y. Jin, Phys. Lett. A **218**, 94 (1996).
[16] G. A. Kourouklis, A. Jayaraman, and L. G. Van Uitert, Mater. Lett. **5**, 116 (1987).
[17] M. Maczka, W. Paraguassu, A. G. Souza Filho, P. T. C. Freire, J. Mendes Filho, and J. Hanuza, Phys. Rev. B **77**, 094137 (2008).
[18] M. Maczka, P. T. C. Freire, C. Luz-Lima, W. Paraguassu, J. Hanuza, and J. Mendes Filho, J. Phys.: Condens. Matter **22**, 015901 (2010).
[19] J. D. Gale, J. Chem. Soc., Faraday Trans. **93**, 629 (1997).
[20] E. Dowty, Phys. Chem. Miner. **14**, 67 (1987).
[21] M. Maczka, W. Paraguassu, A. G. Souza Filho, P. T. C. Freire, F. E. A. Melo, J. Mendes Filho, and J. Hanuza, J. Raman Spectrosc. **36**, 56 (2005).
[22] G. D. Saraiva, W. Paraguassu, M. Maczka, P. T. C. Freire, J. A. Lima, C. W. A. Paschoal, J. Mendes Filho, and A. G. Souza Filho, J. Raman Spectrosc. **39**, 937 (2008).
[23] M. Maczka, J. Hanuza, W. Paraguassu, A. G. Souza Filho, P. T. C. Freire, and J. Mendes Filho, Appl. Phys. Lett. **92**, 112911 (2008).
[24] M. Maczka, L. Macalik, and J. Hanuza, J. Raman Spectrosc. **40**, 2099 (2009).